WILEY Journal of Applied Polymer Science

On The Use Of Ball Milling To Develop PHBV-Graphene Nanocomposites (I) – Morphology, Thermal Properties And Thermal Stability

Journal:	*Journal of Applied Polymer Science*
Manuscript ID:	APP-2014-12-4258
Wiley - Manuscript type:	Research Article
Keywords:	biodegradable, biomaterials, Biopolymers & renewable polymers, nanotubes, graphene and fullerenes, composites

50x50mm (300 x 300 DPI)

On The Use Of Ball Milling To Develop PHBV-Graphene Nanocomposites (I) – Morphology, Thermal Properties And Thermal Stability

Jesús Ambrosio-Martín[a], Giuliana Gorrasi[b]*, Amparo Lopez-Rubio[a], María José Fabra[a], Luís Cabedo Mas[c], Miguel Angel López-Manchado[d], and Jose María Lagaron[a]*

[a]Novel Materials and Nanotechnology Group, IATA, CSIC, Av. Agustín Escardino 7, 46980 Paterna (Valencia), Spain.

[b]Department of Industrial Engineering University of Salerno, Via Giovanni Paolo II 132, 84084 Fisciano Salerno Italy

[c]ESID, Universitat Jaume I, Avda. Vicent Sos Baynat s/n, 12071 Castellón, Spain

[d]Institute of Polymer Science and Technology, (CSIC), Juan de la Cierva, 3, 28006 Madrid, Spain

*Authors to whom correspondence can be addressed.

Tel: +34 963900022

Tel: +39 089964146

Abstract

In the first part of this work, novel nanocomposites based on poly (3-hydroxybutyrate-co-3-hydroxyvalerate) (PHBV) and functionalized graphene nanosheets (FGS) were prepared through ball milling. As revealed by morphological characterization, this blending methodology was able to allow proper nanofiller dispersion and distribution into the matrix. Thermal properties were studied under non-isothermal and isothermal conditions and the addition of FGS into PHBV matrix, although no changes in crystallization mechanism were observed, it modified the crystallization kinetics leading to increased crystallinity. Thermal stability analysis revealed that FGS affected the mechanism of oxidative thermal degradation and had no effect on thermal degradation by pyrolysis. Furthermore, an analysis of isothermal degradation kinetics showed that FGS speeded up the degradation rate. The Sestak-Berggren model was used as a model to explain the isothermal degradation behaviour of the obtained materials in good agreement with the experimental data.

Keywords: graphenes, nanocomposites, ball milling, polyhydroxyalkanoates

1. Introduction

The massive use of petroleum-based polymers has resulted in environmental concerns derived not only from waste management issues, but also from their low degradation rates. As a result, there is a growing interest in the development of renewable and biodegradable materials to partially replace the oil-based ones. Alternatives such as polyhydroxyalkanoates (PHAs) have sparked great interest due to their biodegradable, biocompatible and renewable features. PHAs can be produced in different ways, i.e. chemically or biologically through fermentation from feedstock. This family comprises mainly the homopolymer, polyhydroxybutyrate (PHB), which has been extensively studied since it presents mechanical properties similar to those of conventional petroleum-based polymers, relatively good thermal properties and high stiffness due to its high crystallinity degree[1]. However, although high crystallinity is useful for some applications, the high stiffness limits its usage in other commercial applications. Moreover, another drawback of this polymer is its low thermal stability, making it unstable during melt processing and also limiting its applicability[2]. Several strategies have been developed to overcome these drawbacks, including blending with other polymers, such as poly (vinyl alcohol) (PVA)[3], polypropylene glycol (PPG)[4] and poly-ε-caprolactone (PCL)[5] or modification of the homopolymer by incorporation of different monomer types during the fermentation process. Copolymerization with hydroxyvalerate (HV) results in poly(3-hydroxybutyrate-co-3-hydroxyvalerate) (PHBV) which has improved mechanical and thermal properties, since incorporation of HV reduces the crystallinity, thus decreasing stiffness and brittleness, and also reducing the melting point without decreasing the thermal stability of the material, although greater improvements in this parameter are still needed[1, 6] . However, reduction in crystallinity is widely known to affect the barrier properties of materials to low molecular weight

substances, which is a key property of materials intended to be used in packaging applications[7, 8]. Because of that, PHBV copolymers still present several drawbacks including high cost, relative brittleness and thermal instability, which had hampered the widespread usage of this family of polymers. As a strategy to improve biopolymer performance, many studies have focussed on the development of composites and, especially, nanocomposites using a variety of fillers. Natural fibres such as kenaf fibres have been incorporated into PHBV matrix achieving significant improvements in mechanical properties[9]. Furthermore, the addition of cellulose nanowhiskers resulted in significant improvements in thermal, mechanical and barrier properties, as well as in thermal stability[1]. Apart from natural organic fillers, lamellar inorganic reinforcing fillers, including nanoclays or double layered hydroxides, among others, have been widely studied, giving rise to materials with improved mechanical, barrier and thermal stability properties[10-13]. It is noteworthy that the improved performance of nanocomposites is achieved, not only by using the inherent properties of the nanofiller, but more importantly by optimizing the dispersion, interface chemistry and nanoscale morphology[14]. Great interest has recently arisen about carbonaceous nanofillers such as carbon nanotubes and carbon nanosheets due to their excellent mechanical, thermal and electrical properties. Several works have been published about the effect of carbon nanotubes in polymer matrices[15-19], and more specifically in PHBV matrix[20-24]. Graphene, another carbon-filler material which is the elementary structure of graphite, composed of one atomic thick layer of sp^2-bonded carbon atoms arranged in a honey comb structure, has emerged in last years. The interest in this specific nanofiller derives not only from its excellent mechanical strength, electrical and thermal conductivity, but also from its high surface area and, thus, high barrier effect on polymer matrices[25, 26]. Therefore, its inherent physical properties along with its lamellar structure have made it

excellent reinforcing nanofiller for polymer and biopolymer nanocomposites[27]. It has been, for instance used as a filler in many polymer matrices such as poly (lactic acid) (PLA)[26, 28], PVA[29], polyethylene (PE)[30] and polystyrene (PS)[31] among others, improving their barrier, mechanical and electrical properties. Recent works have also incorporated low contents of graphene sheets in PHBV matrices through solution casting methods improving, in the same way, the final properties of the obtained materials[6, 32].

The ball milling technique is an alternative and efficient method to produce novel composites with high performances since during the milling "intimate mixing" is promoted[17, 33]. It is considered a novel compounding method and it is based in a high-energy grinding technique, able to induce several mechano-chemical changes in the materials. This technique has been previously used in the development of clay-based and carbon nanotubes-based nanocomposites[17, 34-36]. Moreover, graphene-based nanocomposites have also been synthesized by ball milling since the high energy milling induces graphite delamination, thus improving the final properties of the obtained materials[37]. An effective grafting of polystyrene matrix (PS) onto the surface of graphene sheets using ball milling was reported. With this aim, graphite nanoplatelets were used as initial material, corroborating the effectiveness of its mechano-chemical characteristic of this technique[38]. To the best of our knowledge, the high energy ball milling technique has not been used up to date to develop PHBV-graphene nanocomposites. Because of that, the aim of this work was to evaluate the ball milling technique capacity for the production of PHBV-graphene nanocomposites and the study of the final properties of the so-obtained materials. It has been previously reported that when graphene is functionalized, single-sheet graphene is expected to serve as nanofiller in nanocomposites applications, as functional sites will favor interactions

with the matrix[39]. Because of that, a derivative graphene material such as functionalized graphene sheets was used attempting to optimize the filler-matrix compatibilization. This paper is the first part of a wide work in which we aimed to prepare novel PHVB-graphene nanocomposites using mechanical energy. We analysed morphological organization, through SEM and TEM analysis. We conducted a detailed study of behaviour in the molten state of PHVB as function of filler content, either in isothermal or in non-isothermal conditions. We also analysed the degradation behaviour of PHVB, either in inert atmosphere or in air, depending on graphene content.

2. Experimental Section

2.1 Materials

The bacterial polyhydroxyalkanoate grade was purchased from Goodfellow Cambridge Limited, UK, in pellet form (density 1.25 g cm^{-3}). The supplied material was a melt-processable semicrystalline thermoplastic PHBV12 (polyhydroxybutyrate with 12 mol% of valerate and containing 10 wt% of the plasticizer citric ester) copolymer made by biological fermentation from renewable carbohydrate feedstocks. Prior to the ball milling process, the material was purified by dissolution in chloroform and subsequent precipitation by drop-wise addition to an excess of methanol. The material, in this way, was transformed from pellet to powder form which was necessary for the ball milling process.

Functionalized graphene sheets (FGS) were synthesized by thermal reduction of graphite oxide at 1000°C for 30 s under air atmosphere. Briefly, graphite powder (purum powder < 0.1 mm, Sigma Aldrich) was dispersed in 20 mL of fuming nitric acid

for 20 min; next, potassium chlorate (8 g) was slowly added over 1 h and the reaction mixture was stirred for 21 h at 0°C. Graphene produced through this method leads to the formation of single graphene layers or stacks of up to 7 sheets with hydroxyl, carbonyl and epoxy groups on their surface[39]. A full description of the synthesis and characterization of the FGS can be found elsewhere[40].

2.2 Sample Preparation (High Energy Ball Milling - HEBM)

FGS and PHBV powder were milled in the solid state in a Retsch (Germany) centrifugal ball mill (model PM100). The milling process was carried out in a cylindrical steel jar of 50 cm^3 with 5 steel balls of 10 mm of diameter. The rotation speed used was 650 rpm and the milling time was fixed to 60 min. In these experimental conditions, six series of composites PHBV-FGS with 0.1, 0.5, 1.0, 1.5, 2.0, and 3.0 wt% of FGS were prepared. An additional PHBV sample without filler to be taken as a reference was also milled in the same conditions. The PHBV-FGS mixtures and the pure milled PHBV were molded in a hot press (Carver Inc.) at 175ºC giving rise to 250±50 μm thick films. Preparation of the PHBV/FGS nanocomposites is shown in Figure 1.

2.3 Characterization

2.3.1 Scanning Electron Microscopy (SEM)

For scanning electron microscopy (SEM) observation, the samples were cryofractured after immersion in liquid nitrogen, mounted on bevel sample holders and sputtered with Au/Pd in a vacuum. The experiments were conducted on a Hitachi microscope (Hitachi

S-4100) at an accelerating voltage of 10 KV and a working distance of 12−16 mm taking pictures for the sample thickness.

2.3.2 Transmission Electron Microscopy (TEM)

Transmission electron microscopy (TEM) was performed using a JEOL 1010 (Jeol, Tokyo, Japan) equipped with a digital Bioscan (Gatan) image acquisition system. TEM observations were performed on ultrathin sections of microtomed thin composite sheets.

2.3.3 Differential Scanning Calorimetry (DSC)

Thermal properties of PHBV and its nanocomposites with FGS were evaluated by DSC using a DTA Mettler Toledo (DSC 30) under nitrogen atmosphere. The analysis was carried out on samples with a mass ranging between 10 and 12 mg. The samples were heated from 0ºC to 180ºC at 10ºC/min. To ensure reliability of the data obtained, heat flow and temperature were calibrated with standard materials, indium, and zinc. The degree of crystallinity was calculated by taking the specific heat of fusion of perfectly crystalline PHBV. For materials with HV contents equal or higher than 10 mol%, the classical value reported was used, $\Delta H_m^o = 109$ J g^{-1}[141].

In addition, the isothermal crystallization kinetics experiments were evaluated at different temperatures. The samples were heated to 180ºC and annealed at that temperature for 10 min to eliminate the thermal history of any specimen. After that, the samples were cooled rapidly at 100ºC/min, to the desired crystallization temperatures, T_c, ensuring that the crystallization process did not start during the cooling step. Finally, the temperature was held until crystallization was complete. The exothermic crystallization peaks were recorded as a function of time at T_c.

2.3.4 Thermogravimetric Analysis (TGA)

Thermogravimetric analysis (TGA) was carried out with a Mettler TC-10 thermobalance. The samples were heated from 25°C to 800°C at 10 °C/min heating rate under air flow and nitrogen flow. The weight loss was recorded as function of temperature. Moreover, isothermal thermogravimetric analysis was performed in nitrogen environment for pure PHBV and its composites with 0.5, 1.5 and 3 wt%. The temperature was raised from room temperature to 100ºC at 75ºC/min and kept for 3 minutes to eliminate the water. From 100ºC to the respective isothermal degradation temperature, T_d, the temperature was raised at 100ºC/min heating rate. After that, the sample was subjected to T_d for a predetermined time.

3. Results And Discussion

3.1 Morphological Characterization

In order to study the dispersion of the FGS within the PHBV matrix, SEM and TEM experiments were carried out. Figure 2 shows the cryofractured sections of the neat PHBV and its nanocomposite films. Homogeneous dispersion and distribution of the filler, which appears as laminar structures, was observed, especially at low contents. When the amount of FGS increased, although the filler was randomly dispersed, filler concentration areas were noticed. Moreover, while the neat polymer showed a rather flat, clean and smooth fracture surface due to the known brittleness of PHBV[42, 43], as the FGS content increased, the materials exhibited less homogeneous and rougher fractured

surfaces with more irregularities. This effect has also been reported when high concentration of graphene was incorporated into poly (vinylidene fluoride)[44] or polylactide (PLA)[45]. Figure 3 shows TEM micrographs of PHBV-FGS nanocomposites with high and low FGS content. These images further confirm the good filler dispersion in PHBV matrix as well as the fact that the filler was concentrated in certain areas for highly loaded nanocomposites. Consequently, the ball milling technique seems to be an appropriate tool to obtain a homogeneous distribution of FGS within the PHBV biopolymeric matrix, especially at low content.

3.2 Melting And Crystallization Behaviour Of PHBV And Its Nanocomposites

With the aim of investigating the effects of the FGS addition on the thermal properties of the PHBV nanocomposites, DSC analyses of all samples were carried out. The melting temperatures (T_m) and melting enthalpy (ΔH_m) normalized to the PHBV content of the nanocomposite films were evaluated from the DSC first and second heating runs. The degree of crystallinity (X_c) was only calculated from the DSC first heating run and crystallization temperature (T_c) and crystallization enthalpy (ΔH_c) were also obtained from DSC cooling run. Table 1 gathers all the DSC data for PHBV and its nanocomposites.

As shown in Figure 4, neat PHBV displays multiple melting peaks in the first heating, which occurred between 150°C and 180ºC. Multiple melting peaks behaviour of PHBV copolymer was interpreted previously as an effect of the melting-recrystallization process occurring during subsequent heating[46]. During the slow heating scans, less perfect crystals have sufficient time to melt and reorganize into more perfectly structured crystals which lead to this bimodal melting peak behaviour, as reported. The

reorganized crystals are then subsequently re-melted at higher temperatures[47]. In line with these statements, Owen et al.[48] pointed out that the low-temperature melting peak was probably related to heterogeneous nucleation of PHBV which started spontaneously by PHBV chain aggregation below the melting point forming less perfect crystals and the high temperature melting peak was related to homogeneous nucleation of PHBV. Addition of low amounts of FGS into PHBV matrix did not result in big changes on the low melting temperature. However, at high contents, an increase in the low melting temperature peak was observed. This allows to hypothesize that the fraction of crystals that melted at lower temperatures was composed by bigger or more perfect crystals if compared with the neat polymer. On the other hand, the high melting peak temperature remained almost unaltered for the PHBV nanocomposites in regard to neat polymer. These results differ to some extent with previous studies about the incorporation of graphene[6] nanoclays[49, 50] or carbon nanotubes[24] into PHVB, where a decrease in the melting temperature peak was observed as the nanofiller concentration was increased. In spite of this, an analysis of the ratio of the melting peak areas demonstrated that at low FGS content there was an increase of the fraction of more perfect or larger crystals which remained more or less constant up to 1 wt% (cf. Figure 5). This fraction was then dramatically reduced when high contents of FGS were introduced within the PHBV matrix. This could indicate that high contents of FGS hindered the crystallization process to some extent generating more defective crystals or high loadings created more heterogeneous materials since there were more nucleation sites which induced PHBV crystallization. This result is consistent with the fact that the first melting peak could be related to heterogeneous nucleation, as previously observed. A reduction of the second melting peak area relative to the first melting peak area was also observed when MWCNT were incorporated into PHBV biopolymer[23, 24].

From Table 1, it can be seen that the melting enthalpy values increased at each PHBV-FGS composition when compared with neat biopolymer, which was associated to a slight increase in the crystallinity degree. However, the maximum crystallinity degree was obtained for the nanocomposite containing 1 wt% FGS. For higher nanofiller loading, although crystallinity was still higher than that for the pure polymer, the crystallization degree underwent a slight decrease. This is in accordance with the data reported in the melting peak areas study where high FGS contents were considered to hinder the crystallization process to some extent. The increase in crystallinity could be ascribed to the nucleating effect of the FGS which increased the nucleation rate of PHBV and thus, improved the overall crystallization rate, as previously reported for PHBV nanocomposites containing graphene[6], multiwalled carbon nanotubes[21] or cellulose nanowhiskers[51]. Moreover, it was reported that well-dispersed multi-walled carbon nanotubes led to an increased number of sites available for nucleation, thereby enhancing the crystallization rate of PHBV[20]. Therefore, DSC results are consistent with SEM observations where, although no agglomerates were observed for high loadings, filler concentration areas could be observed, which could hinder the nucleation effect to some extent and hence, generating lower crystallization degree than that obtained for lower loadings.

Regarding the cooling process, which is related with the non-isothermal crystallization behaviour of the PHBV-nanocomposites, a clear trend of increased crystallization temperature with the increase in FGS content was observed, corroborating the nucleating effect of FGS. In addition, the crystallization peaks of nanocomposites become slightly sharper, which was directly associated with the non-isothermal crystallization rate[23], there being an acceleration of the non-isothermal crystallization process in the presence of FGS. The crystallization enthalpy of the nanocomposites was

generally higher than that of pure polymer, as shown in Table 1. However, at high FGS contents, it decreased to values close to that for pure PHBV. Once again, it could be observed that high FGS contents hinder the crystallization process, as mentioned above. Only one melting peak was obtained in the second heating scan with a melting temperature between the low and high temperature melting peaks observed in the first heating run. Moreover, small shoulder was observed at higher temperatures. For the samples with 2 and 3 wt% FGS content, sharper melting peaks were obtained and the shoulder became smaller, almost disappearing. This indicates that, after a controlled cooling process, the polymer chains were able to crystallize in a more stable and homogeneous way. Furthermore, the melting enthalpies were higher than in the first heating run, indicating that a higher crystalline fraction was generated after the controlled cooling process.

The isothermal crystallization kinetics of PHBV and its nanocomposites were investigated in order to obtain further information about the effect of FGS addition on the crystallization process of PHBV. The crystallization exothermic peaks of PHBV and its nanocomposites at different temperatures (T_i), 133°C, 135°C and 137ºC were analyzed. As an example, Figure 6 shows the crystallization peaks of neat PHBV, and the nanocomposites containing 1 wt% and 3 wt% FGS at those temperatures. From this figure it can be stated that the crystallization process occurred more slowly with increasing T_i and it became shorter with addition of FGS. The crystallization kinetics of neat PHBV and its nanocomposites was analysed by the well established model for isothermal crystallization, i.e. the Avrami model.

$$X_t = 1 - \exp(-Kt^n) \quad (1)$$

where X_t is the relative degree of crystallinity after crystallization time t, n is the Avrami exponent which is related to the type of nucleation mechanism and to the geometry of

the growing crystals, and K is the overall (macroscopic) kinetics rate constant (it contains contributions from both nucleation and growth).

A derivative method reported by De Santis and Pantani[52] was used to directly fit the calorimetric curve of the isothermal crystallization process to the derivative form of the Avrami equation. The data obtained from the Avrami fitting is compiled in Table 2. The half-time of crystallization $t_{½}$ is defined as the time required to reach 50% of the total crystallinity and was calculated from the values of n and K[52]. The determination of the crystallization half-time under isothermal conditions is an interesting method to provide clear-cut evidence of the effectiveness of nucleating agents on polymer matrices[53]. In fact, it is also used to directly characterize the crystallization rate, since the reciprocal half-time of crystallization ($1/ t_{½}$) can be considered approximately proportional to the crystal growth rate[54]. Thus, it can be observed that the shorter half-time of crystallization the higher the crystallization rate. Data in Table 2 demonstrated that the values of the overall crystallization rate constant increased as the FGS content increased. At the same time, $t_{½}$ parameter decreased with addition of FGS. Therefore, an acceleration of the crystallization process took place when FGS was incorporated. Regarding the Avrami exponent, it was not altered with the FGS incorporation, indicating that the crystallization mechanism was probably the same. In fact, for all the samples a bimodal melting peak was observed suggesting that the same crystallization mechanism occurred. As mentioned above, the low-temperature melting peak was probably related to heterogeneous nucleation of PHBV and the high temperature melting peak was related to homogeneous nucleation of PHBV. The effect of increasing the crystallization rate with increasing nanofiller concentration is also in agreement with the non-isothermal crystallization study carried out by DSC where an acceleration of the crystallization process was observed due to the FGS nucleating effect.

Therefore, it could be concluded that although there were no changes in the crystallization mechanism, the presence of FGS had an effect on the kinetics and dynamics of PHBV crystallization. The well dispersed FGS altered the crystallization rate and the crystal size and shape, accelerating the crystallization process and giving rise to bigger and more heterogeneous crystallites. Similar effect has been reported for nanocomposites of PHBV and MWCNT[20, 23]. These effects were strongly dependent on the FGS content. Thus, for high FGS content, the crystallization process was somehow hindered, generating more defective and/or smaller crystals when compared with the nanocomposites with lower FGS content. In contrast, increasing the FGS content led to a greater nucleating effect of FGS, showing an increase in the crystallization temperature, which was directly related with the non-isothermal crystallization rate, and also an increase in the isothermal crystallization rate.

3.3 Thermal Stability Of PHBV And Its Nanocomposites

The thermal stability of the neat PHBV and PHBV-FGS nanocomposites were analysed using TGA. Thermal degradation temperatures, onset temperatures and the residues at 400 and 800ºC were evaluated and the results are presented in Table 3. Figure 7 shows the TGA curves of graphene, PHBV and PHBV-FGS nanocomposites. It is clearly observed a better thermal stability of FGS than that for the neat polymer and polymer nanocomposites in both air and nitrogen environment. All nanocomposites showed similar degradation behaviour if compared to neat polymer. However, despite the high thermal stability of the FGS, while for nitrogen environment there was no change on the thermal degradation temperature of PHBV matrix with FGS addition, a decrease was noticed when thermal stability was analysed in the presence of air. In this case, the

greater the FGS content the lower the thermal degradation temperature observed for the nanocomposite. Moreover, onset degradation temperatures shifted to lower temperatures with increasing FGS, unlike in nitrogen environment, where they remained more or less constant. Therefore, it seems that addition of FGS affected the mechanism of oxidative thermal degradation of PHBV while had no effect on thermal degradation by pyrolysis. Indeed, it was observed that for pure FGS different degradation mechanism took place in presence of air or nitrogen. Polymers loaded with layered nanofillers, such as layered silicates, layered double hydroxide or layered metallic phosphate usually exhibit an increased thermal stability being attributed to the mass and heat barrier effects that this kind of fillers infer to the matrix[28]. In this case, although graphene can be considered a good mass barrier for volatile degradation products, it has high heat conductivity. Therefore, the decrease in degradation temperature can be ascribed to the low heat barrier effect of graphene in polymer composites. In fact, a recent study reported that PLA-graphene nanocomposites could be ignited with less heat irradiation than the pristine polymer. The reason of that was the high heat conductivity of graphene which allowed easier and faster heat diffusion through the matrix[28]. A small shoulder was observed around 500ºC for all PHBV-FGS nanocomposites in both air and nitrogen environment, except for 0.1 wt%. Attending to the degradation curve of pure graphene, the mass loss at this point could be attributed to the degradation of graphene present in the nanocomposite. Focusing on this high temperature area of the graph, it was observed that there was a direct and accurate relationship between the mass loss after 400ºC and the FGS content of the nanocomposites both in air and nitrogen environments (cf. Table 3). Moreover, higher thermal degradation temperatures were observed when the experiments were performed under nitrogen atmosphere, which is in accordance with the higher thermal stability of FGS in these conditions.

The isothermal degradation kinetics of PHBV and PHBV-FGS at 0.5 wt%, 1.5 wt% and 3 wt% nanocomposites were investigated at predetermined temperatures, 230°C, 240°C and 250ºC in order to further study the effect of FGS addition on the degradation process of PHBV. The weight loss profiles of PHBV and its nanocomposites during isothermal heating at the established temperatures are shown in Figure 8a. A normal one step isothermal degradation process is observed, where higher isothermal degradation temperatures produced faster weight loss. Moreover all composites could speed up the degradation rate of pristine matrix at any determined degradation temperature since the establishments of constant mass plateau were shifted to lower degradation times compared with pure PHBV, i.e., reducing its thermal stability, as observed by TGA.

To evaluate the kinetics of the degradation process, it was assumed that the weight loss during degradation process was associated with the depolymerization reaction. Thus, the degree of depolymerization can be defined as:

$$\alpha = \frac{m_0 - m_t}{m_0 - m_f} \quad (2)$$

With m_0 is the initial weight, m_t is the weight at any time and m_f is the weight at the end of the degradation process.

To describe the kinetic of polymer degradation, a single step kinetic equation is normally used.

$$\frac{d\alpha}{dt} = k(T) f(\alpha) \quad (3)$$

where $k(T)$ is a temperature dependent rate constant which is expressed as Arrhenius type equation, i.e, $k(T)=A \cdot exp(-E_a/RT)$, with A and E_a the pre-exponential factor and activation energy respectively, and $f(\alpha)$ expresses the reaction model which describe dependence of the reaction rate on the extent of reaction. Different expressions of $f(\alpha)$ for the most frequently used mechanism are proposed in the literature[12, 55, 56]. The

general form of n[th]-order of $f(\alpha)$ is $f(\alpha)=(1-\alpha)^n$. Figure 8b shows the $d\alpha/dt$ as a function of degree of depolymerisation, α, for PHBV and its nanocomposites at different temperatures. There was non-linear relationship between $d\alpha/dt$ and α, and thus, the simple first-order kinetic model (n=1) could not be used as a model to explain the isothermal degradation behaviour of these materials. On the contrary, the peak profiles of the data plots were in the form of a parabola. This non-linear dependence of the kinetics degradation model with de depolymerization degree of PHB incorporating different kinds of nanofillers has been previously reported[12, 55-57], where a contribution of further reactions mechanism such as autocatalytic reactions or chain scission mechanism were proposed. Moreover, it has been reported that the kinetics degradation model of PHBV does not follow simple first-order kinetics. A more complex degradation process was considered involving degradation of different compounds with different decomposition rates[58].

To understand the degradation reaction of our materials, Sestak-Berggren (Equation. 4) model was used to adjust our isothermal degradation data.

$$\frac{d\alpha}{dt} = k(1-\alpha)^n \alpha^m \quad (4)$$

The relative values of n and m determine relative contributions from decay and acceleratory regions of the thermal degradation process, respectively. This model is known as autocatalytic model and is considered one of the more satisfactory models to describe the observed phenomena[12, 57]. As observed in Figure 8, there was good agreement between the experimental data and the model prediction for pure polymer and for any composition at the various isothermal degradation temperatures. The fitting parameters k, n, m were obtained and are reported in Table 4 along with the correlation factor of the fitting. As observed from this table, an increment in the degradation rate constant was observed for the nanocomposites when compared with the neat PHBV at

each temperature. This again indicates reduction in the thermal stability of the obtained nanocomposites. Furthermore the acceleratory reaction of thermal degradation was larger than decay reaction ($m > n$) for each material at each temperature. These results confirmed the ability of autocatalytic degradation model as a good general model to describe the degradation of PHBV and its nanocomposites with FGS. In order to evaluate the well known "kinetic triplet", i.e, A, E_a and $f(\alpha)$, the Arrhenius equation was transformed to its logarithmic form and the Arrhenius plots of ln(k) vs 1/T were achieved. The pre-exponential factor and activation energy were calculated from slope and intercept of the linear fitting respectively (cf. Figure 9). A reduction in the activation energy was observed when the FGS content increased. This indicated that lower energy was necessary to start the degradation process, which was reflected in the increase of the isothermal degradation kinetic rate constant and hence in the thermal degradation rate.

4. Conclusions

In this work PHBV-functionalized graphene sheets (FGS) nanocomposites were successfully obtained through the ball milling technique and the effect of FGS addition was studied. The morphological characterization revealed good dispersion of the filler which was also well distributed, although for high loadings, filler concentration areas were observed. Isothermal and non-isothermal crystallization analysis confirmed that addition of FGS did not lead to changes in the crystallization mechanism. However, an effect in the crystallization rate and in the crystal shape was observed. FGS was seen to act as a nucleating agent, increasing the overall crystallization rate and the crystallization degree but generating more heterogeneous crystals. It was demonstrated that these effects were strongly dependent on the FGS content. Furthermore, a decrease

in thermal stability was observed, especially under air conditions, mainly ascribed to the low heat barrier effect of the FGS which made heat diffusion easier and faster through the matrix. This work provides evidence that the ball milling technique can be successfully applied to develop graphene-based nanocomposites with good dispersion and distribution of the filler into the polymer matrix.

Acknowledgements

J Ambrosio-Martín would like to thank the Spanish Ministry of Economy and Competitiveness for the FPI grant BES-2010-038203. M.J. Fabra is recipient of a "Juan de la Cierva" contract from the Spanish Ministry of Economy and Competitiveness. The authors acknowledge financial support from the MINECO (MAT2012-38947-C02-01 project) and from the FP7 ECOBIOCAP project.

References

1. Martínez-Sanz, M.; Villano, M.; Oliveira, C.; Albuquerque, M. G. E.; Majone, M.; Reis, M.; Lopez-Rubio, A.; Lagaron, J. M., *New Biotechnol.* **2014**, 31, 364-376.

2. Pardo-Ibáñez, P.; Lopez-Rubio, A.; Martínez-Sanz, M.; Cabedo, L.; Lagaron, J. M., *J. Appl. Polym. Sci.* **2014**, 131,

3. Yoshie, N.; Azuma, Y.; Sakurai, M.; Inoue, Y., *J. Appl. Polym. Sci.* **1995**, 56, 17-24.

4. Roa, J. P. B.; De O. Patrício, P. S.; Oréfice, R. L.; Lago, R. M., *J. Appl. Polym. Sci.* **2013**, 128, 3019-3025.

5. Hinüber, C.; Häussler, L.; Vogel, R.; Brünig, H.; Heinrich, G.; Werner, C., *Express Polym. Lett.* **2011**, 5, 643-652.

6. Sridhar, V.; Lee, I.; Chun, H. H.; Park, H., *Express Polym. Lett.* **2013**, 7, 320-328.

7. Guinault, A.; Sollogoub, C.; Domenek, S.; Grandmontagne, A.; Ducruet, V., *Int. J. Mate. Form.* **2010**, 3, 603-606.

8. Drieskens, M.; Peeters, R.; Mullens, J.; Franco, D.; Lemstra, P. J.; Hristova-Bogaerds, D. G., *J. Polym. Sci, Part B: Polym. Phys.* **2009**, 47, 2247-2258.

9. Russo, P.; Carfagna, C.; Cimino, F.; Acierno, D.; Persico, P., *Adv. Polym. Technol.* **2013**, 32, E313-E322.

10. Dagnon, K. L.; Chen, H. H.; Innocentini-Mei, L. H.; D'Souza, N. A., *Polym. Int.* **2009**, 58, 133-141.

11. Sanchez-Garcia, M. D.; Lagaron, J. M., *J. Appl. Polym. Sci.* **2010**, 118, 188-199.

12. Achilias, D. S.; Panayotidou, E.; Zuburtikudis, I., *Thermochim. Acta.* **2011**, 514, 58-66.

13. Sorrentino, A.; Gorrasi, G.; Vittoria, V. In Environmental Silicate Nano-Biocomposites; Avérous, L.; Pollet, E., Eds.; Springer London, **2012**, Chap. 9, pp 237-264

14. Ramanathan, T.; Abdala, A. A.; Stankovich, S.; Dikin, D. A.; Herrera-Alonso, M.; Piner, R. D.; Adamson, D. H.; Schniepp, H. C.; Chen, X.; Ruoff, R. S.; Nguyen, S. T.; Aksay, I. A.; Prud'Homme, R. K.; Brinson, L. C., *Nat. Nanotechnol.* **2008**, 3, 327-331.

15. Gorrasi, G.; Bredeau, S.; Candia, C. D.; Patimo, G.; Pasquale, S. D.; Dubois, P., *Polym. Adv. Technol.* **2012**, 23, 1435-1440.

16. Gorrasi, G.; Bredeau, S.; Di Candia, C.; Patimo, G.; De Pasquale, S.; Dubois, P., *Macromol. Mater. Eng.* **2011**, 296, 408-413.

17. Gorrasi, G.; Sarno, M.; Di Bartolomeo, A.; Sannino, D.; Ciambelli, P.; Vittoria, V., *J. Polym. Sci, Part B: Polym. Phys.* **2007**, 45, 597-606.

18. Ouyang, C.; Luo, J.; Wang, Y.; Zhang, Z., *Lizi Jiaohuan Yu Xifu/Ion Exchange and Adsorption* **2012**, 28, 343-351.

19. Dottori, M.; Armentano, I.; Fortunati, E.; Kenny, J. M., *J. Appl. Polym. Sci.* **2011**, 119, 3544-3552.

20. Lai, M.; Li, J.; Yang, J.; Liu, J.; Tong, X.; Cheng, H., *Polym. Int.* **2004**, 53, 1479-1484.

21. Shan, G. F.; Gong, X.; Chen, W. P.; Chen, L.; Zhu, M. F., *Colloid. Polym. Sci.* **2011**, 289, 1005-1014.

22. Yu, H. Y.; Yao, J. M.; Qin, Z. Y.; Liu, L.; Yang, X. G., *J. Appl. Polym. Sci.* **2013**, 130, 4299-4307.

23. Ma, Y.; Zheng, Y.; Wei, G.; Song, W.; Hu, T.; Yang, H.; Xue, R., *J. Appl. Polym. Sci.* **2012**, 125, E620-E629.

24. Vidhate, S.; Innocentini-Mei, L.; D'Souza, N. A., *Polym. Eng. Sci.* **2012**, 52, 1367-1374.

25. Jiang, X.; Drzal, L. T., *J. Power. Sources.* **2012**, 218, 297-306.

26. Pinto, A. M.; Cabral, J.; Tanaka, D. A. P.; Mendes, A. M.; Magalhães, F. D., *Polym. Int.* **2013**, 62, 33-40.

27. Verdejo, R.; Bernal, M. M.; Romasanta, L. J.; Lopez-Manchado, M. A., *J. Mater. Chem.* **2011**, 21, 3301-3310.

28. Bao, C.; Song, L.; Xing, W.; Yuan, B.; Wilkie, C. A.; Huang, J.; Guo, Y.; Hu, Y., *J. Mater. Chem.* **2012**, 22, 6088-6096.

29. Wang, J.; Wang, X.; Xu, C.; Zhang, M.; Shang, X., *Polym. Int.* **2011**, 60, 816-822.

30. El Achaby, M.; Qaiss, A., *Mater. Des.* **2013**, 44, 81-89.

31. Stankovich, S.; Dikin, D. A.; Dommett, G. H. B.; Kohlhaas, K. M.; Zimney, E. J.; Stach, E. A.; Piner, R. D.; Nguyen, S. T.; Ruoff, R. S., *Nature* **2006**, 442, 282-286.

32. Wang, B. J.; Zhang, Y. J.; Zhang, J. Q.; Gou, Q. T.; Wang, Z. B.; Chen, P.; Gu, Q., *Chinese Journal of Polymer Science (English Edition)* **2013**, 31, 670-678.

33. Shaw, W. J. D., *Mater. Sci. Forum* **1998**, 269-272, 19-30.

34. Gorrasi, G.; Piperopoulos, E.; Lanza, M.; Milone, C., *J. Phys. Chem. Solids* **2013**, 74, 1-6.

35. Vertuccio, L.; Gorrasi, G.; Sorrentino, A.; Vittoria, V., *Carbohydr. Polym.* **2009**, 75, 172-179.

36. Perrin-Sarazin, F.; Sepehr, M.; Bouaricha, S.; Denault, J., *Polym. Eng. Sci.* **2009**, 49, 651-665.

37. Wu, H.; Zhao, W.; Chen, G., *J. Appl. Polym. Sci*. **2012**, 125, 3899-3903.

38. Wu, H.; Zhao, W.; Hu, H.; Chen, G., *J. Mater. Chem.* **2011**, 21, 8626-8632.

39. Schniepp, H. C.; Li, J. L.; McAllister, M. J.; Sai, H.; Herrera-Alonson, M.; Adamson, D. H.; Prud'homme, R. K.; Car, R.; Seville, D. A.; Aksay, I. A., *J. Phys. Chem. B* **2006**, 110, 8535-8539.

40. Verdejo, R.; Barroso-Bujans, F.; Rodriguez-Perez, M. A.; De Saja, J. A.; Lopez-Manchado, M. A., *J. Mater. Chem.* **2008**, 18, 2221-2226.

41. Branciforti, M. C.; Corrêa, M. C. S.; Pollet, E.; Agnelli, J. A. M.; Nascente, P. A. D. P.; Avérous, L., *Polym. Test.* **2013**, 32, 1253-1260.

42. Horng, Y. T.; Chien, C. C.; Huang, C. T.; Wei, Y. H.; Chen, S. Y.; Lan, J. C. W.; Soo, P. C., *Biochem. Eng. J.* **2013**, 78, 73-79.

43. Wang, X.; Chen, Z.; Chen, X.; Pan, J.; Xu, K., *J. Appl. Polym. Sci.* **2010**, 117, 838-848.

44. El Achaby, M.; Arrakhiz, F. Z.; Vaudreuil, S.; Essassi, E. M.; Qaiss, A.; Bousmina, M., *J. Appl. Polym. Sci.* **2013**, 127, 4697-4707.

45. Kim, I. H.; Jeong, Y. G., *J. Polym. Sci, Part B: Polym. Phys.* **2010**, 48, 850-858.

46. Gunaratne, L. M. W. K.; Shanks, R. A., *Eur. Polym. J.* **2005**, 41, 2980-2988.

47. Jiang, L.; Morelius, E.; Zhang, J.; Wolcott, M.; Holbery, J., *J. Compos. Mater.* **2008**, 42, 2629-2645.

48. Owen, A. J.; Heinzel, J.; Škrbić, Ž.; Divjaković, V., *Polymer* **1992**, 33, 1563-1567.

49. Wang, S.; Song, C.; Chen, G.; Guo, T.; Liu, J.; Zhang, B.; Takeuchi, S., *Polym. Degrad. Stab.* **2005**, 87, 69-76.

50. Bittmann, B.; Bouza, R.; Barral, L.; Diez, J.; Ramirez, C., *Polym. Compos.* **2013**, 34, 1033-1040.

51. Ten, E.; Jiang, L.; Wolcott, M. P., *Carbohydr. Polym.* **2012**, 90, 541-550.

52. De Santis, F.; Pantani, R., *J. Therm. Anal. Calorim.* **2013**, 112, 1481-1488.

53. Goffin, A. L.; Raquez, J. M.; Duquesne, E.; Siqueira, G.; Habibi, Y.; Dufresne, A.; Dubois, P., *Biomacromolecules* **2011**, 12, 2456-2465.

54. Mensitieri, G.; Di Maio, E.; Buonocore, G. G.; Nedi, I.; Oliviero, M.; Sansone, L.; Iannace, S., *Trends Food Sci. Tech.* **2011**, 22, 72-80.

55. Erceg, M.; Kovačić, T.; Klarić, I., *Thermochim. Acta* **2009**, 485, 26-32.

56. Erceg, M.; Kovačić, T.; Sanja, P., *Polym. Compos.* **2010**, 31, 272-278.

57. Wu, T. M.; Hs, S. F.; Shih, Y. F.; Liao, C. S., *J. Polym. Sci, Part B: Polym. Phys.* **2008**, 46, 1207-1213.

58. Cyras, V. P.; Vázquez, A.; Rozsa, C.; Galego Fernández, N.; Torre, L.; Kenny, J. M., *J. Appl. Polym. Sci.* **2000**, 77, 2889-2900

Figures

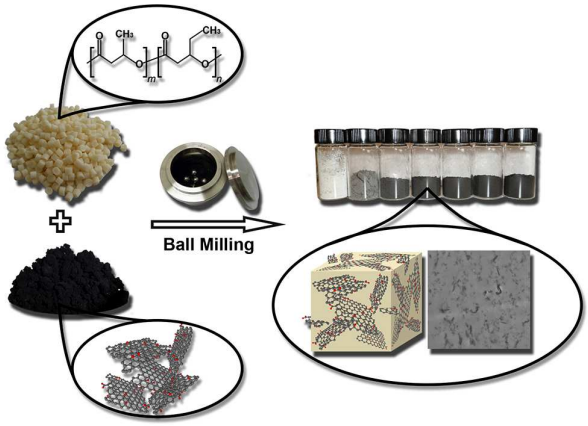

Figure 1. Preparation of PHBV/FGS nanocomposites.

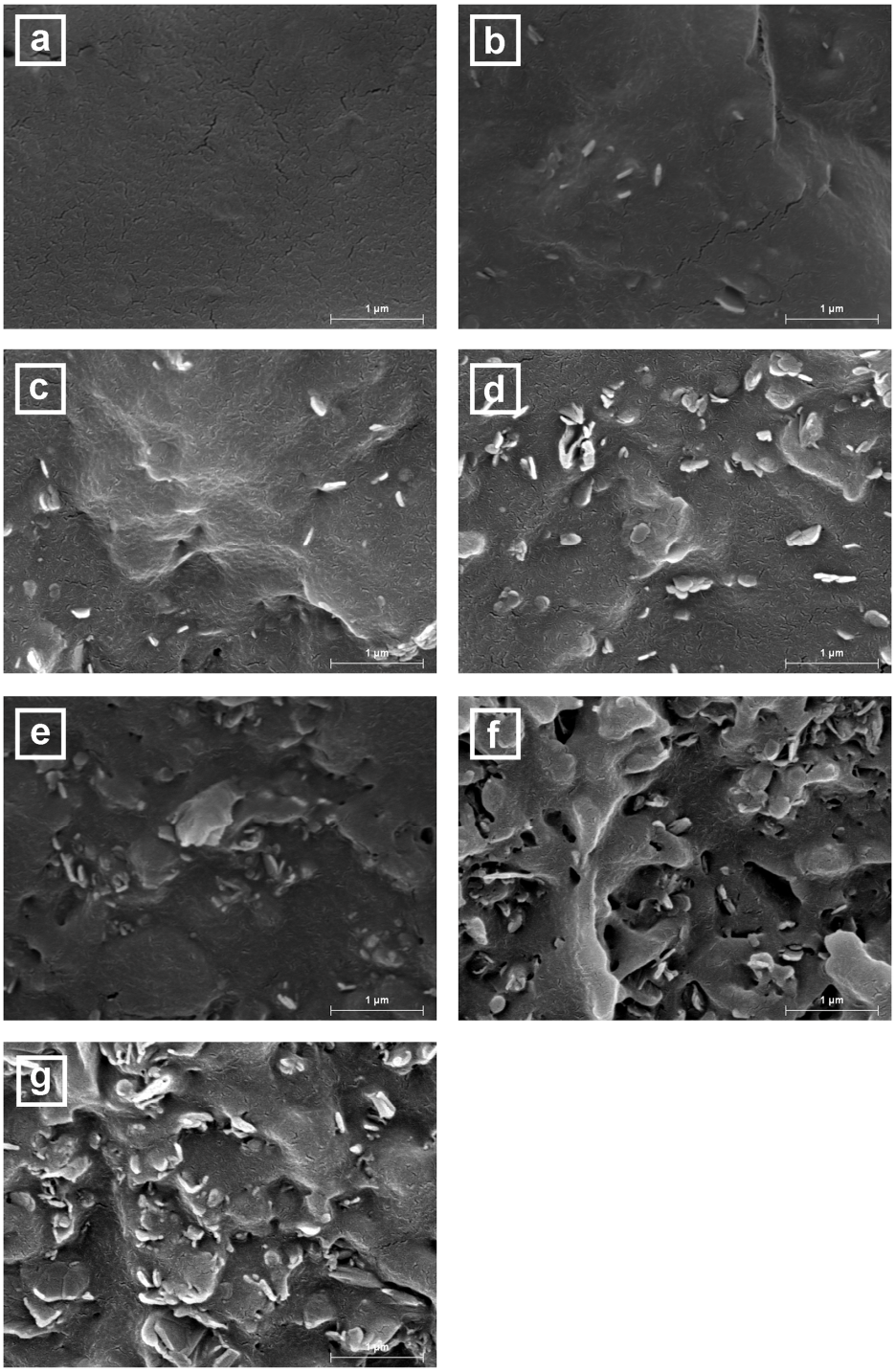

Figure 2. SEM micrographs of the cryo-fractured sections of pure PHBV (a) and PHBV-FGS nanocomposites films at 0.1 wt% (b); 0.5 wt% (c); 1.0 wt% (d); 1.5 wt% (e); 2.0 wt% (f) and 3.0 wt% (g). Scale markers correspond to 1µm.

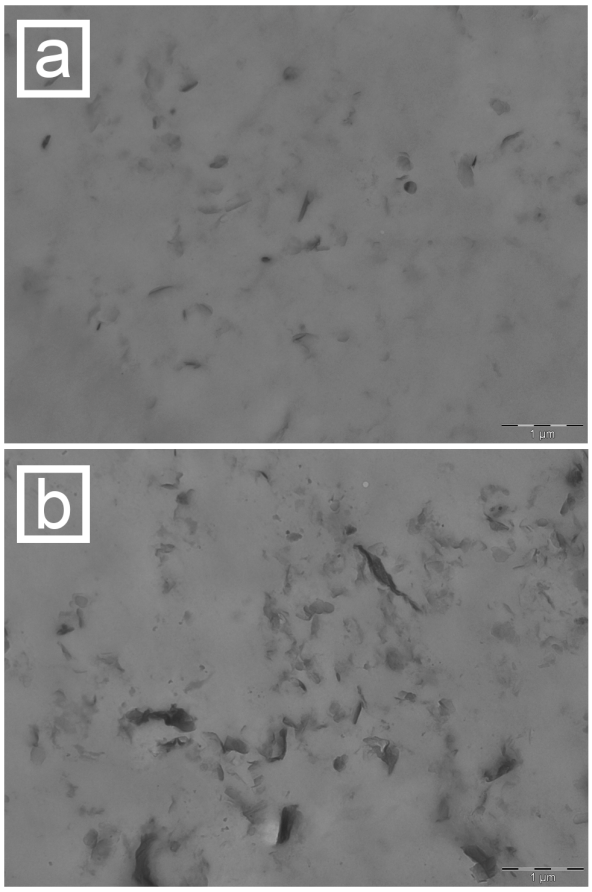

Figure 3. TEM micrographs of PHBV-FGS films containing 0.5 wt% FGS (a) and 2.0 wt% FGS (b). Scale markers correspond to 1µm.

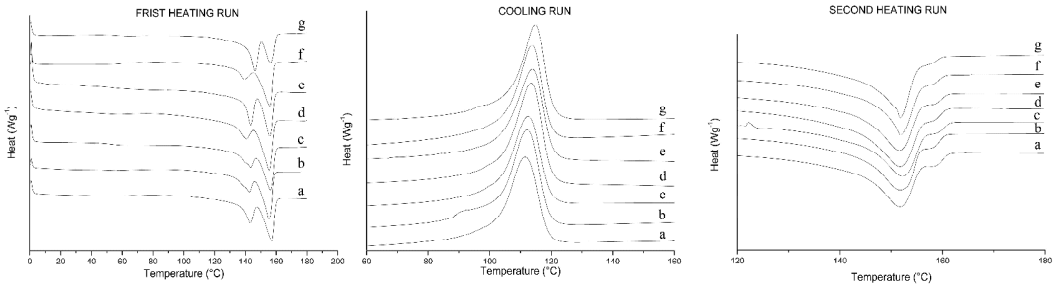

Figure 4. DSC thermograms of first heating, cooling and second heating runs of pure PHBV (a) and PHBV-FGS nanocomposites at 0.1 wt% (b); 0.5 wt% (c); 1.0 wt% (d); 1.5 wt% (e); 2.0 wt% (f) and 3.0 wt% (g).

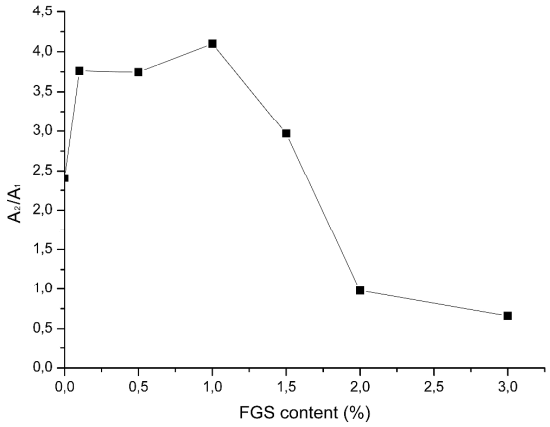

Figure 5. Melting peaks areas ratio as function of FGS content. A_1 and A_2 are the areas of the lower and higher melting temperature peaks, respectively.

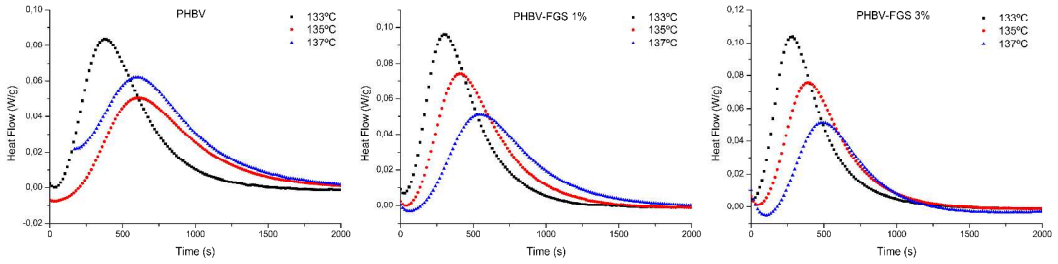

Figure 6. DSC experimental curves during isothermal crystallization study of PHBV and its nanocomposites with 1.0 wt% and 3.0 wt% FGS.

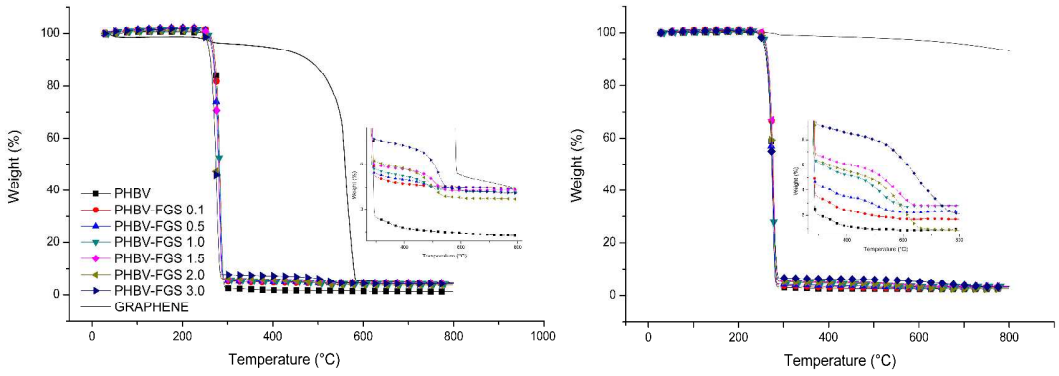

Figure 7. TGA curves of pure FGS, pure PHBV and its nanocomposites with FGS in air environment (left) and nitrogen environment (right).

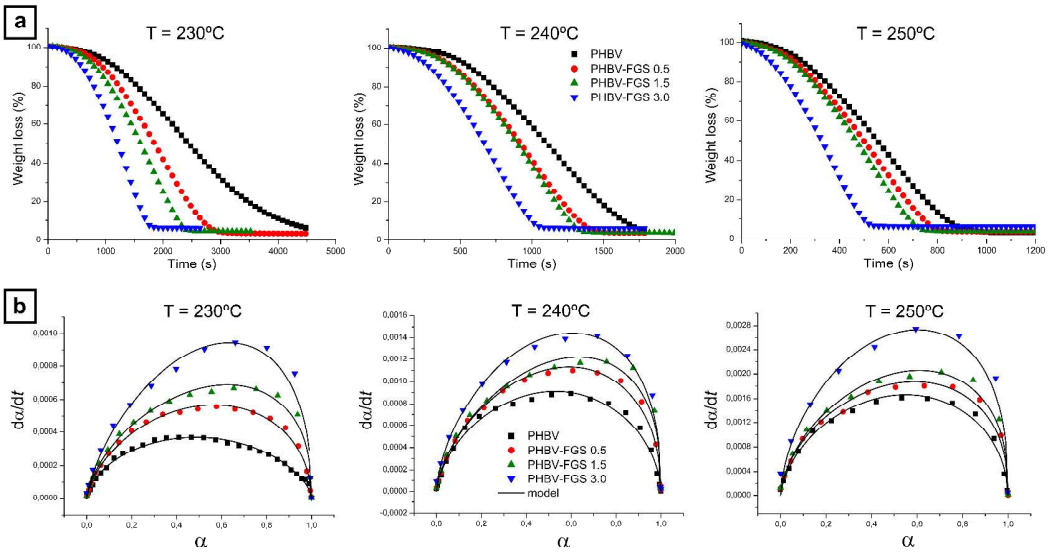

Figure 8. Weight loss profiles versus time (a) and the experimental and calculated data using the Sestak Berggren model of dα/dt versus α (b) of PHBV and its nanocomposites with 0.5 wt%, 1.0 wt% and 3.0 wt% FGS at 230ºC, 240ºC and 250ºC isothermal temperatures.

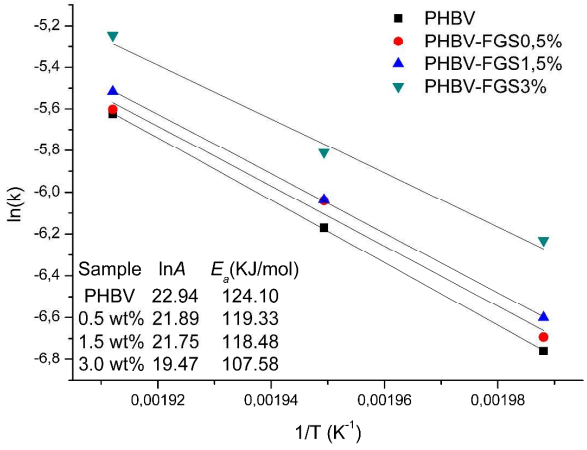

Figure 9. Arrhenius plots of ln(*k*) versus 1/T for PHBV and PHBV-FGS nanocomposites.

Table 1. DSC glass transition temperature (T_{g1}), maximum of melting (T_m), melting enthalpy (ΔH_m), during the first heating run, crystallization temperature (T_c), crystallization enthalpy (ΔH_c), during the cooling run, and maximum of melting (T_m) and melting enthalpy (ΔH_m) during second heating run.

	First Heating				Cooling		Second Heating	
	T_{m1} (ºC)	T_{m2} (ºC)	ΔH_m (J/g)	Xc (%)	T_c (ºC)	ΔH_c (J/g)	T_m (ºC)	ΔH_m (J/g)
PHBV	143.3	157.5	58.0	53.2	111.2	62.9	152.0	68.6
PHBV-FGS 0,1 %	142.5	155.5	64.9	59.5	112.0	69.9	151.8	70.0
PHBV-FGS 0,5 %	143.5	156.5	63.8	58.5	112.2	68.0	152.3	70.1
PHBV-FGS 1 %	141.7	155.8	74.6	68.4	113.2	69.9	152.0	76.9
PHBV-FGS 1,5 %	142.8	156.8	69.8	64.1	113.8	69.9	152.3	81.9
PHBV-FGS 2 %	148.3	158.3	63.5	58.3	114.2	62.5	154.0	71.9
PHBV-FGS 3 %	146.3	156.5	63.1	57.9	114.7	64.0	152.0	72.7

Table 2. The values of kinetic rate constant (*K)*, Avrami exponent (*n)*, and half-time of crystallization ($t_{1/2)}$ as function of crystallization temperature of PHBV and its nanocomposites.

Temperature (ºC)	TRG content (wt%)	$K \times 10^3$ (s^{-1})	*n*	$t_{1/2}$ (s)
130	0	2,5	1,6	318,1
	0.1	2,6	1,6	309,6
	0.5	2,7	1,5	293,2
	1.0	2,9	1,6	270,7
	1.5	2,8	1,7	290,3
	2.0	3,2	1,6	244,6
	3.0	3,3	1,5	240,1
135	0	1,8	1,6	443,0
	0.1	2,1	1,7	383,9
	0.5	2,2	1,7	361,2
	1.0	2,4	1,6	330,7
	1.5	2,5	1,6	320,4
	2.0	2,7	1,6	297,2
	3.0	2,6	1,7	303,5
137	0	1,6	1,7	511,9
	0.1	1,6	1,7	495,9
	0.5	1,8	1,8	454,7
	1.0	1,9	1,6	410,9
	1.5	2,0	1,6	394,9
	2.0	2,1	1,7	385,4
	3.0	2,5	1,8	328,9

Table 3. TGA decomposition temperatures (T_d), onset temperature and the difference between % residue at 400ºC and 800ºC of PHBV and its nanocomposites incorporating FGS evaluated in air and nitrogen environment.

	Air				Nitrogen			
	T_{d1} (ºC)	T_{d2} (ºC)	On-set (ºC)	$R_{400ºC} - R_{800ºC}$ (%)	T_{d1} (ºC)	T_{d2} (ºC)	On-set (ºC)	$R_{400ºC} - R_{800ºC}$ (%)
PHBV	284.2	-	269.3	0.2	276.6	-	259.6	0.1
PHBV-FGS 0,1 %	282.3	-	266.2	0.3	278.3	-	262.4	0.3
PHBV-FGS 0,5 %	280.0	472.8	263.7	0.7	276.1	495.9	259.3	0.6
PHBV-FGS 1 %	279.9	483.5	259.0	1.1	277.6	511.8	258.9	1.2
PHBV-FGS 1,5 %	278.9	508.5	263.3	1.4	278.4	558.0	262.0	1.6
PHBV-FGS 2 %	273.8	500.4	257.4	2.0	276.6	580.7	257.9	2.3
PHBV-FGS 3 %	273.4	522.3	257.0	3.1	275.5	645.2	255.3	3.2

Table 4. Fitting parameters of Sestak-Berggren model to the isothermal degradation data.

Temperature	Sample	*k*	*n*	*m*	R^2
230	PHBV	11.6 e^{-4}	0.616	0.582	0.98
	PHBV-FGS 0,5 %	12.4 e^{-4}	0.492	0.645	0.99
	PHBV-FGS 1,5 %	13.6 e^{-4}	0.385	0.646	0.98
	PHBV-FGS 3 %	19.7 e^{-4}	0.412	0.708	0.98
240	PHBV	20.9 e^{-4}	0.563	0.634	0.99
	PHBV-FGS 0,5 %	23.8 e^{-4}	0.452	0.651	0.99
	PHBV-FGS 1,5 %	23.9 e^{-4}	0.376	0.651	0.97
	PHBV-FGS 3 %	28.7 e^{-4}	0.404	0.620	0.98
250	PHBV	36.1 e^{-4}	0.507	0.619	0.98
	PHBV-FGS 0,5 %	36.9 e^{-4}	0.412	0.591	0.98
	PHBV-FGS 1,5 %	40.2 e^{-4}	0.390	0.610	0.98
	PHBV-FGS 3 %	52.8 e^{-4}	0.388	0.591	0.97

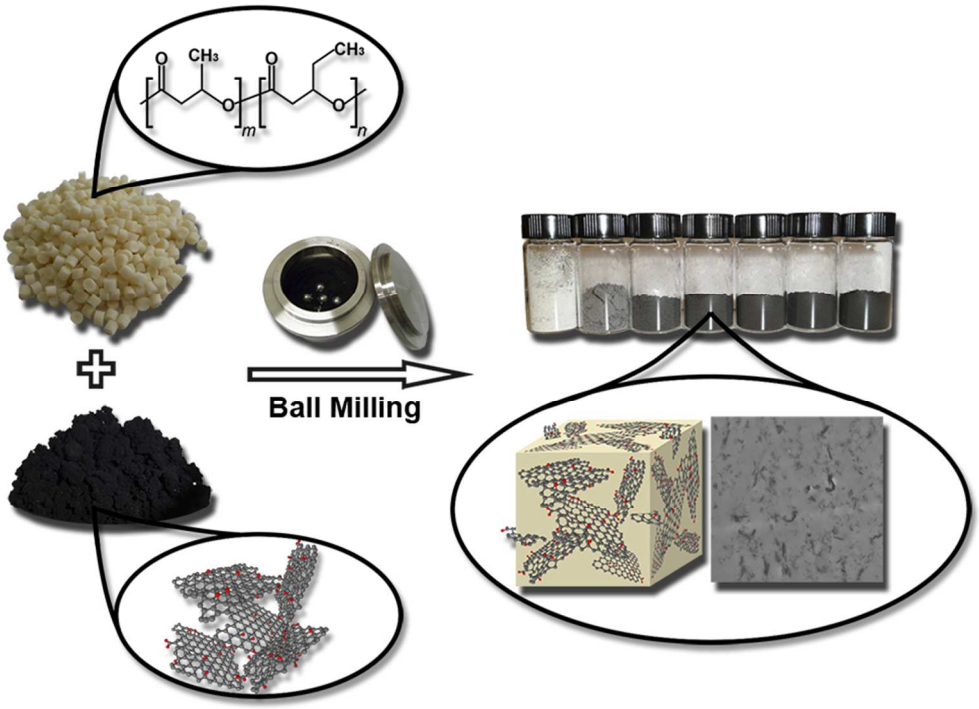

Figure 1. Preparation of PHBV/FGS nanocomposites.
83x62mm (300 x 300 DPI)

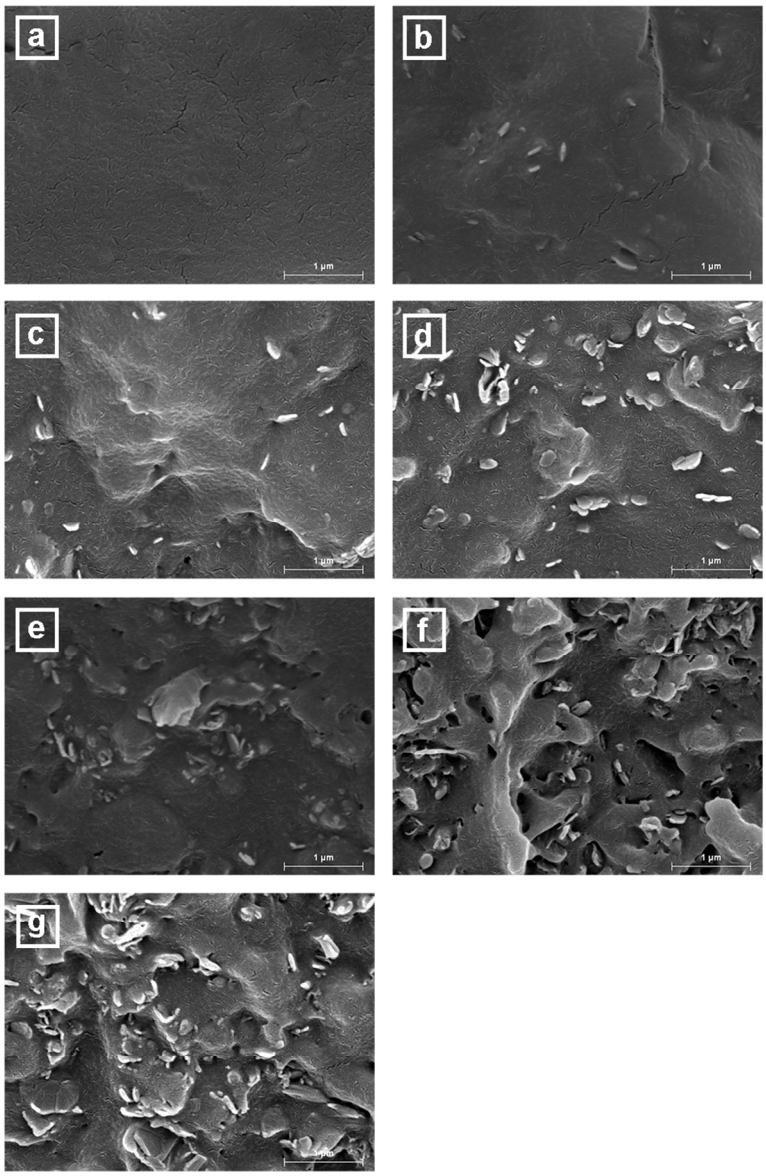

Figure 2. SEM micrographs of the cryo-fractured sections of pure PHBV (a) and PHBV-FGS nanocomposites films at 0.1 wt% (b); 0.5 wt% (c); 1.0 wt% (d); 1.5 wt% (e); 2.0 wt% (f) and 3.0 wt% (g). Scale markers correspond to 1µm.
83x127mm (300 x 300 DPI)

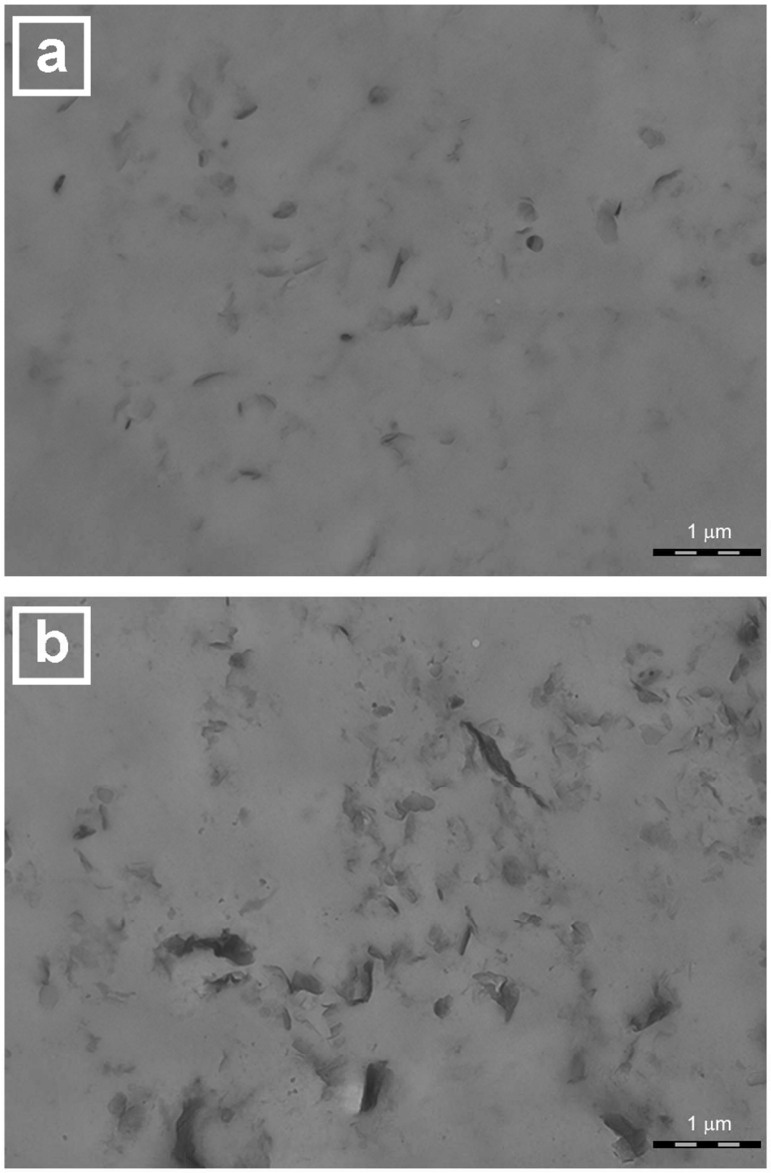

Figure 3. TEM micrographs of PHBV-FGS films containing 0.5 wt% FGS (a) and 2.0 wt% FGS (b). Scale markers correspond to 1μm.
83x126mm (300 x 300 DPI)

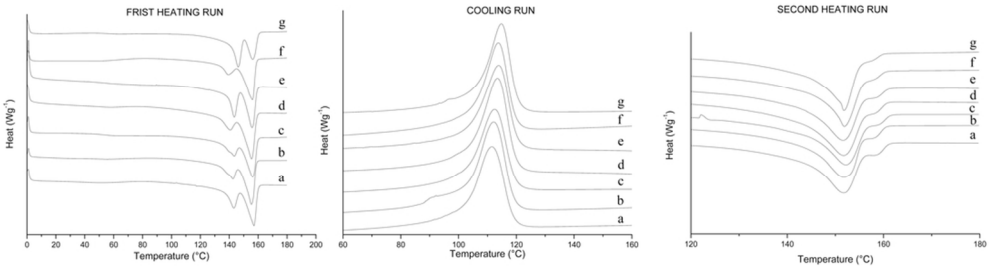

Figure 4. DSC thermograms of first heating, cooling and second heating runs of pure PHBV (a) and PHBV-FGS nanocomposites at 0.1 wt% (b); 0.5 wt% (c); 1.0 wt% (d); 1.5 wt% (e); 2.0 wt% (f) and 3.0 wt% (g).
46x12mm (600 x 600 DPI)

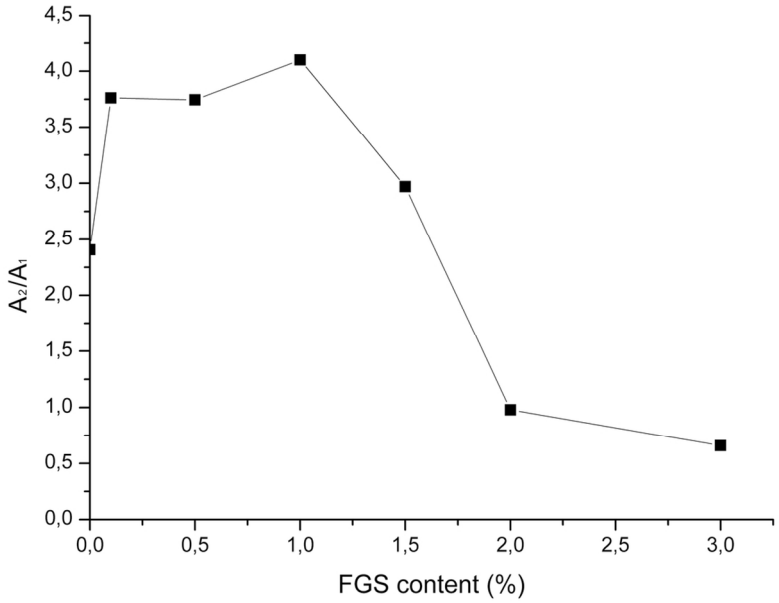

Figure 5. Melting peaks areas ratio as function of FGS content. A1 and A2 are the areas of the lower and higher melting temperature peaks, respectively.
58x41mm (600 x 600 DPI)

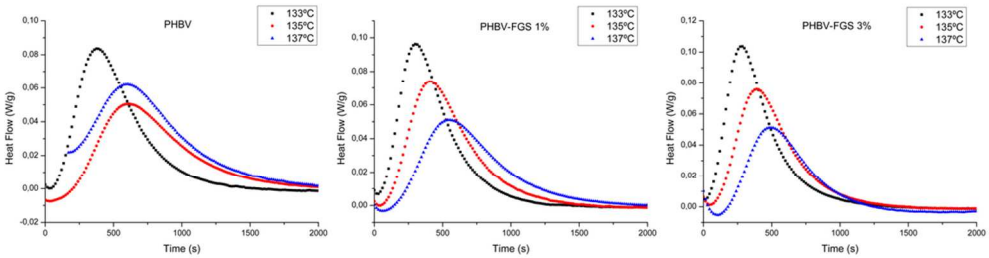

Figure 6. DSC experimental curves during isothermal crystallization study of PHBV and its nanocomposites with 1.0 wt% and 3.0 wt% FGS.
48x13mm (600 x 600 DPI)

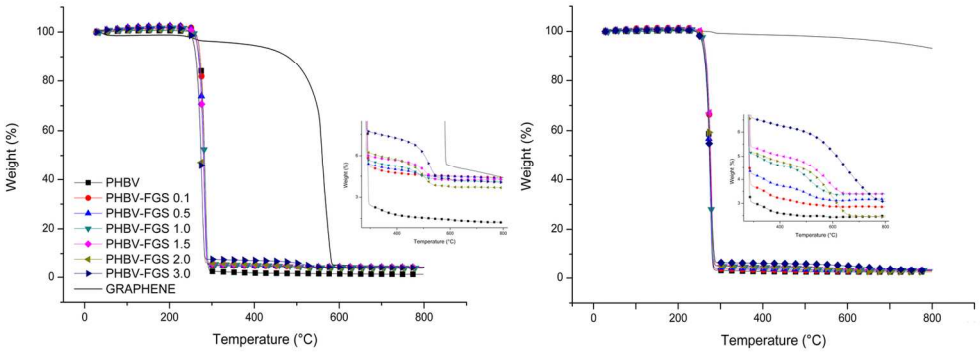

Figure 7. TGA curves of pure FGS, pure PHBV and its nanocomposites with FGS in air environment (left) and nitrogen environment (right).
71x29mm (600 x 600 DPI)

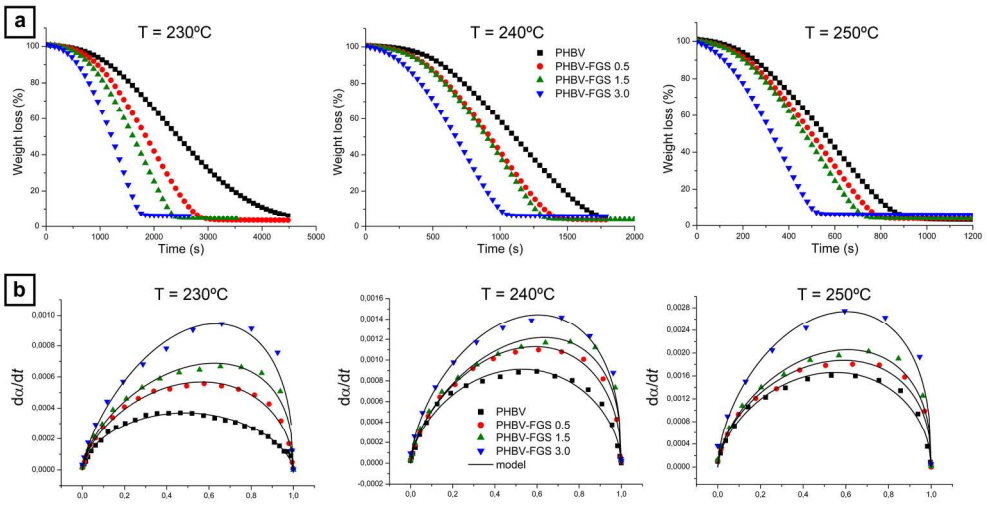

Figure 8. Weight loss profiles versus time (a) and the experimental and calculated data using the Sestak Berggren model of dα/dt versus α (b) of PHBV and its nanocomposites with 0.5 wt%, 1.0 wt% and 3.0 wt% FGS at 230ºC, 240ºC and 250ºC isothermal temperatures.
92x49mm (600 x 600 DPI)

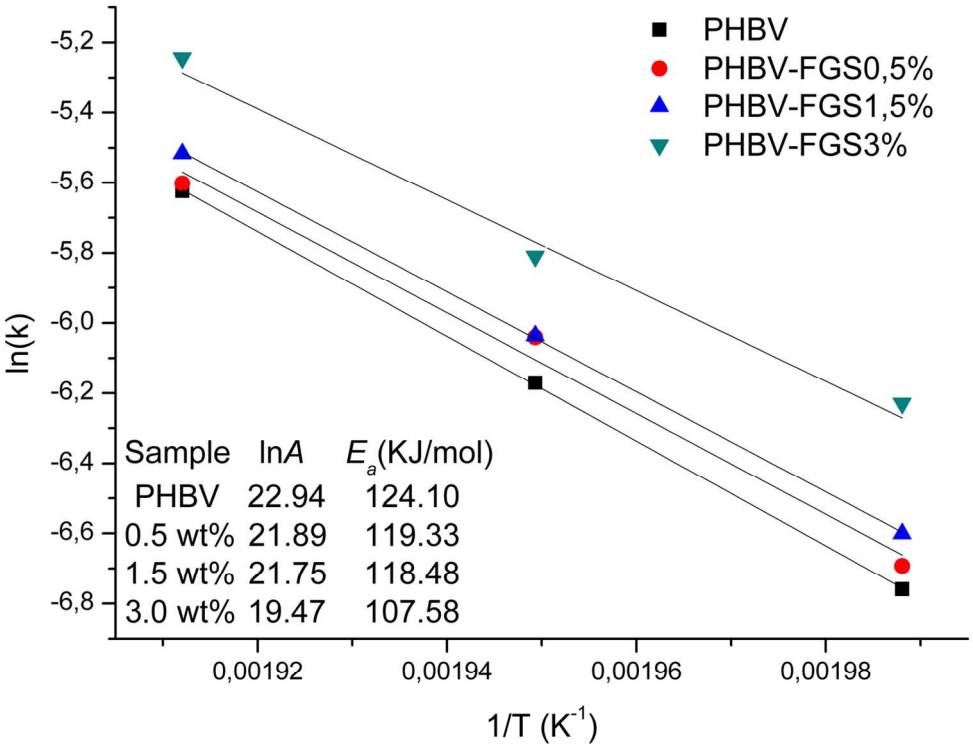

Figure 9. Arrhenius plots of ln(k) versus 1/T for PHBV and PHBV-FGS nanocomposites.
65x51mm (600 x 600 DPI)

Table 1. DSC glass transition temperature (T_{g1}), maximum of melting (T_m), melting enthalpy (ΔH_m), during the first heating run, crystallization temperature (T_c), crystallization enthalpy (ΔH_c), during the cooling run, and maximum of melting (T_m) and melting enthalpy (ΔH_m) during second heating run.

	First Heating				Cooling		Second Heating	
	T_{m1} (ºC)	T_{m2} (ºC)	ΔH_m (J/g)	Xc (%)	T_c (ºC)	ΔH_c (J/g)	T_m (ºC)	ΔH_m (J/g)
PHBV	143.3	157.5	58.0	53.2	111.2	62.9	152.0	68.6
PHBV-FGS 0,1 %	142.5	155.5	64.9	59.5	112.0	69.9	151.8	70.0
PHBV-FGS 0,5 %	143.5	156.5	63.8	58.5	112.2	68.0	152.3	70.1
PHBV-FGS 1 %	141.7	155.8	74.6	68.4	113.2	69.9	152.0	76.9
PHBV-FGS 1,5 %	142.8	156.8	69.8	64.1	113.8	69.9	152.3	81.9
PHBV-FGS 2 %	148.3	158.3	63.5	58.3	114.2	62.5	154.0	71.9
PHBV-FGS 3 %	146.3	156.5	63.1	57.9	114.7	64.0	152.0	72.7

Table 2. The values of kinetic rate constant (*K)*, Avrami exponent (*n)*, and half-time of crystallization ($t_{1/2)}$ as function of crystallization temperature of PHBV and its nanocomposites.

Temperature (ºC)	TRG content (wt%)	$K \times 10^3$ (s^{-1})	*n*	$t_{1/2}$ (s)
130	0	2,5	1,6	318,1
	0.1	2,6	1,6	309,6
	0.5	2,7	1,5	293,2
	1.0	2,9	1,6	270,7
	1.5	2,8	1,7	290,3
	2.0	3,2	1,6	244,6
	3.0	3,3	1,5	240,1
135	0	1,8	1,6	443,0
	0.1	2,1	1,7	383,9
	0.5	2,2	1,7	361,2
	1.0	2,4	1,6	330,7
	1.5	2,5	1,6	320,4
	2.0	2,7	1,6	297,2
	3.0	2,6	1,7	303,5
137	0	1,6	1,7	511,9
	0.1	1,6	1,7	495,9
	0.5	1,8	1,8	454,7
	1.0	1,9	1,6	410,9
	1.5	2,0	1,6	394,9
	2.0	2,1	1,7	385,4
	3.0	2,5	1,8	328,9

Table 3. TGA decomposition temperatures (T_d), onset temperature and the difference between % residue at 400ºC and 800ºC of PHBV and its nanocomposites incorporating FGS evaluated in air and nitrogen environment.

	Air				Nitrogen			
	T_{d1} (ºC)	T_{d2} (ºC)	On-set (ºC)	$R_{400ºC} - R_{800ºC}$ (%)	T_{d1} (ºC)	T_{d2} (ºC)	On-set (ºC)	$R_{400ºC} - R_{800ºC}$ (%)
PHBV	284.2	-	269.3	0.2	276.6	-	259.6	0.1
PHBV-FGS 0,1 %	282.3	-	266.2	0.3	278.3	-	262.4	0.3
PHBV-FGS 0,5 %	280.0	472.8	263.7	0.7	276.1	495.9	259.3	0.6
PHBV-FGS 1 %	279.9	483.5	259.0	1.1	277.6	511.8	258.9	1.2
PHBV-FGS 1,5 %	278.9	508.5	263.3	1.4	278.4	558.0	262.0	1.6
PHBV-FGS 2 %	273.8	500.4	257.4	2.0	276.6	580.7	257.9	2.3
PHBV-FGS 3 %	273.4	522.3	257.0	3.1	275.5	645.2	255.3	3.2

Table 4. Fitting parameters of Sestak-Berggren model to the isothermal degradation data.

Temperature	Sample	*k*	*n*	*m*	R^2
230	PHBV	11.6 e^{-4}	0.616	0.582	0.98
	PHBV-FGS 0,5 %	12.4 e^{-4}	0.492	0.645	0.99
	PHBV-FGS 1,5 %	13.6 e^{-4}	0.385	0.646	0.98
	PHBV-FGS 3 %	19.7 e^{-4}	0.412	0.708	0.98
240	PHBV	20.9 e^{-4}	0.563	0.634	0.99
	PHBV-FGS 0,5 %	23.8 e^{-4}	0.452	0.651	0.99
	PHBV-FGS 1,5 %	23.9 e^{-4}	0.376	0.651	0.97
	PHBV-FGS 3 %	28.7 e^{-4}	0.404	0.620	0.98
250	PHBV	36.1 e^{-4}	0.507	0.619	0.98
	PHBV-FGS 0,5 %	36.9 e^{-4}	0.412	0.591	0.98
	PHBV-FGS 1,5 %	40.2 e^{-4}	0.390	0.610	0.98
	PHBV-FGS 3 %	52.8 e^{-4}	0.388	0.591	0.97

Figure Captions

Figure 1. Preparation of PHBV/FGS nanocomposites.

Figure 2. SEM micrographs of the cryo-fractured sections of pure PHBV (a) and PHBV-FGS nanocomposites films at 0.1 wt% (b); 0.5 wt% (c); 1.0 wt% (d); 1.5 wt% (e); 2.0 wt% (f) and 3.0 wt% (g). Scale markers correspond to 1μm.

Figure 3. TEM micrographs of PHBV-FGS films containing 0.5 wt% FGS (a) and 2.0 wt% FGS (b). Scale markers correspond to 1μm.

Figure 4. DSC thermograms of first heating, cooling and second heating runs of pure PHBV (a) and PHBV-FGS nanocomposites at 0.1 wt% (b); 0.5 wt% (c); 1.0 wt% (d); 1.5 wt% (e); 2.0 wt% (f) and 3.0 wt% (g).

Figure 5. Melting peaks areas ratio as function of FGS content. A_1 and A_2 are the areas of the lower and higher melting temperature peaks, respectively.

Figure 6. DSC experimental curves during isothermal crystallization study of PHBV and its nanocomposites with 1.0 wt% and 3.0 wt% FGS.

Figure 7. TGA curves of pure FGS, pure PHBV and its nanocomposites with FGS in air environment (left) and nitrogen environment (right).

Figure 8. Weight loss profiles versus time (a) and the experimental and calculated data using the Sestak Berggren model of $d\alpha/dt$ versus α (b) of PHBV and its nanocomposites with 0.5 wt%, 1.0 wt% and 3.0 wt% FGS at 230ºC, 240ºC and 250ºC isothermal temperatures.

Figure 9. Arrhenius plots of $\ln(k)$ versus 1/T for PHBV and PHBV-FGS nanocomposites.

Tables Captions

Table 1. DSC glass transition temperature (T_{g1}), maximum of melting (T_m), melting enthalpy (ΔH_m), during the first heating run, crystallization temperature (T_c), crystallization enthalpy (ΔH_c), during the cooling run, and maximum of melting (T_m) and melting enthalpy (ΔH_m) during second heating run.

Table 2. The values of kinetic rate constant (*K)*, Avrami exponent (*n)*, and half-time of crystallization ($t_{1/2)}$ as function of crystallization temperature of PHBV and its nanocomposites.

Table 3. TGA decomposition temperatures (T_d), onset temperature and the difference between % residue at 400ºC and 800ºC of PHBV and its nanocomposites incorporating FGS evaluated in air and nitrogen environment.

Table 4. Fitting parameters of Sestak-Berggren model to the isothermal degradation data.